Journal of Science and Technology in Civil Engineering, HUCE, 2026, 20 (1): 59–79

MECHANICAL AND THERMAL BUCKLING ANALYSIS OF FUNCTIONALLY GRADED SANDWICH BEAMS WITH FOAM CORE USING DIFFERENT BEAM THEORIES

Duc-Kien Thai[a], Van-Long Nguyen[b,d,*], Minh-Duc Do[c,d], Thanh-Binh Chu[b,d]

[a]*Department of Civil and Environmental Engineering, Sejong University, 209 Neungdong-ro, Gwangjin Gu, Seoul 05006, Republic of Korea*
[b]*Faculty of Industrial and Civil Engineering, Hanoi University of Civil Engineering, 55 Giai Phong road, Bach Mai ward, Hanoi, Vietnam*
[c]*Faculty of Civil Engineering, The University of Da Nang - University of Science and Technology, 54 Nguyen Luong Bang, Lien Chieu Ward, Da Nang, Vietnam*
[d]*Frontier research group of Mechanics of Advanced Materials and Structures (MAMS), Hanoi University of Civil Engineering, 55 Giai Phong road, Bach Mai ward, Hanoi, Vietnam*

Article history:
Received 24/11/2025, Revised 07/3/2026, Accepted 18/3/2026

Abstract

Using various beam theories, this study investigates the buckling of sandwich beams with functionally graded faces and a foam core subjected to either thermal or mechanical loading. The mechanical properties of materials constituting the sandwich beams are tailored to vary smoothly from the bottom to the top surfaces. For thermal buckling, three typical types of temperature distribution are considered: uniform, linear, and nonlinear temperature distributions. The minimum potential energy is employed to derive the governing equations and the trigonometric admissible functions-based Ritz method is adopted to discretize these equations for the approximate solution. A convergence study is performed to determine the appropriate number of terms in the admissible functions. Comparison studies are conducted to validate the results of the current study. In addition, the effects of beam theories, material distribution, slenderness ratio, temperature distributions, porosity coefficient, boundary conditions, and layer thickness ratio on the buckling of the beams are examined. Numerical results reveal that beam theories have a significant influence on the buckling behavior of sandwich beams with a foam core.

Keywords: mechanical and thermal buckling; Ritz method; beam theory; sandwich beam with foam core; functionally graded material.

https://doi.org/10.31814/stce.huce2026-20(1)-05

1. Introduction

In functionally graded materials (FGMs), since the mechanical and physical properties vary smoothly, the stress concentration phenomenon can be eliminated. Moreover, FGMs are often composed of a mixture of ceramic and metal to combine the excellent features of the two constituent materials: ceramic offers excellent resistance to heat and chemical corrosion, while metal provides toughness and strength. Therefore, structures made of FGMs can withstand both high mechanical loads and extreme temperature gradients. These advanced materials have significant potential for use in high-performance structures across various fields, such as spacecraft, nuclear plants, automotive industry, machine elements, etc. [1, 2, 3, 4].

In the design of structures and structural components, buckling is a critical phenomenon that must be addressed to prevent catastrophic failure. Over the past decades, both theoretical and experimental

*Corresponding author. *E-mail address:* longnv@huce.edu.vn (Nguyen, V.-L.)

studies related to this topic have attracted the attention of scientists and engineers. Up to now, there have been a lot of studies on the buckling of single- and multi-layer FGM beams published in the literature, including mechanical buckling [5, 6, 7, 8, 9, 10, 11], thermal buckling [12, 13, 14, 15, 16, 17, 18, 19, 20]. In the aforementioned references, the commonly addressed issues include the buckling loads, buckling temperatures, buckling mode shapes, post-buckling, dynamic buckling, as well as computational methods and beam models.

In the simulation of beam behavior, one-dimensional (1D) modelling is mostly preferred due to its low computational cost compared with 2D or 3D models. Various 1D beam theories have been proposed and successfully applied in beam analysis. The oldest and most well-known theory is the Euler-Bernoulli beam theory, also called the classical beam theory (CBT). This theory simplifies the formulations but overpredicts the load-carrying capacity because shear deformation is neglected. The next theory, proposed by Timoshenko and commonly known as the first-order shear deformation beam theory (FBT), accounts for shear deformation. In FBT, the assumption of constant shear strain over the cross-section is unrealistic; therefore, a shear correction factor is required to compensate for the resulting error. The third group, known as higher-order shear deformation beam theories (HOBTs), overcomes this shortcoming. These theories can accurately capture the transverse shear stress across the beam thickness, and a notable advantage is that no shear correction factor is required. The most recent versions are quasi-3D beam theories, which extend from HOBTs by considering thickness stretching effects. An overview of various beam theories, their mathematical formulations, and applications in the analysis of FGM beams was presented in detail by Sayyad and Ghugal [4].

Three-layer-sandwich beams, in which two FGM faces cover a foam core are abbreviated as FGM-FS beams in this paper, represent a new type of lightweight beam structures. This beam type offers an improved structural performance and integrates many excellent characteristics of foam materials, such as reduced self-weight, lower thermal and electrical conductivities, acoustic insulation, and energy absorption, etc. Therefore, they show great potential for engineering applications and have attracted increasing attention from the scientific community. The mechanical response of FGM-FS beams has been investigated and reported by several authors. For example, Hung and Truong [21] employed various shear deformation theories and Navier's solution to examine the free vibration of the FGM-FS beams resting on the Winkler elastic foundation. Chinh et al. [22] used a third-order beam theory (a type of HOBTs) and proposed a 1D mesh-free model to study the static flexural analysis of the FGM-FS beams. Mu and Zhao [23] analyzed the fundamental frequency of the FGM-FS beams by using the extended Galerkin method. In their work, the classical theory was employed to model the face sheets, whereas a higher-order theory was used for modelling the core. Wang et al. [24] proposed an HOBT to study the transient response of the FGM-FS beams. In their work, the beam was subjected to a non-uniformly distributed moving mass, and the Ritz method was employed to discretize the equations of motion. Hung et al. [25] used Navier's analytical solution to investigate the static behavior of the FGM-FS beams. In their study, the foam core of the beam was infiltrated with water, and the effects of different beam theories on the behavior were investigated. Using the Ritz method with polynomial trial functions and the quasi-3D theory, Hung et al. [26] examined the natural frequencies and forced vibration of the FGM-FS beams in which the foam core was reinforced with graphene platelets (GPLs). Based on an analytical solution and the quasi-3D theory, Wattanasakulpong and Chaikittiratana [27] studied the static bending, fundamental frequency, and mechanical buckling of the FGM-FS beams in which the FGM faces were reinforced with GPLs. Mohamed et al. [28] investigated the natural vibration and buckling of the FGM-FS beams resting on the Pasternak elastic foundation, using the Ritz method and the quasi-3D theory beam model. Eiadtrong et al. [29] focused

on the nonlinear transient responses of FGM-FS beams excited by multiple moving loads, using the Gram-Schmidt-Ritz method and the quasi-3D theory.

The literature survey shows that FGM-FS beams are structural elements that are suitable for applications under heavy loads or thermal environments. However, due to the novelty of these structures, related studies are still limited. Previous works by Hung and Truong [21], and Hung et al. [25] have shown that the selection of beam theory significantly affects the computed vibration and static responses. Nevertheless, its influence on the buckling behavior, particularly on the thermal buckling, has not yet been systematically investigated.

To address this gap, the present paper investigates the mechanical and thermal buckling behavior of FGM-FS beams with the following main contributions:

(a) The thermal bucking behavior of FGM-FS beams is investigated for the first time, which providing novel quantitative and physical insights into the underlying thermal buckling mechanisms.

(b) A systematic comparison of four representative beam theories, namely CBT, FBT, HOBT, and quasi-3D theory, is carried out to clarify the influence of shear deformation and thickness stretching effect on both mechanical and thermal buckling responses.

(c) The effects of key parameters, including material gradation, span-to-height ratio, temperature distribution, porosity coefficient, boundary conditions, and layer thickness ratio, on the mechanical and thermal buckling behavior of FGM-FS beams are examined to elucidate their roles in the buckling behavior and in the relative performance of different beam theories.

The remainder of the paper is organized as follows. Section 2 presents the theoretical framework and fundamental formulations for FGM-FS beams in a thermal environment. Section 3 provides numerical experiments, including convergence studies, model validation, and parametric investigations into the effects of beam theories, temperature distributions, and structural configurations on the mechanical and thermal buckling responses. Finally, Section 4 summarizes the main findings and conclusions.

2. Theoretical and basic formulations

2.1. FGM-FS beams, geometrical parameters, and material properties

Consider FGM-FS beams with length L and a rectangular cross-section of $h \times b$ as shown in Fig. 1. The relationship between the total beam thickness and the thickness of the layers is given by $h = h_c + 2 \times h_f$, where h_c is the core thickness, and h_f denotes the thickness of the face layers. The x-axis of the Cartesian coordinate system is placed on the mid-plane. h_i $(i = 1, 2, 3)$ indicates the coordinate at the surface, in the z-direction, of the layers. Two types of FGM-FS beams are considered in this study: (i) FGM face-functionally graded (FG) foam core-FGM face (defined as FGM-FS I) and (ii) FGM face-FG foam core-isotropic face (defined as FGM-FS II).

a. FGM face-FG foam core-FGM face (FGM-FS I)

This sandwich beam consists of two FGM faces, in which metal and ceramic are mixed together, and an FG porous core made of a metal foam. The mechanical and physical properties, such as Young's modulus E, thermal conductivity coefficient κ, thermal expansion coefficient α, which are generally represented by χ, are defined using the power-law and cosine distribution as [24]

$$\begin{cases} \chi(z) = (\chi_m - \chi_c)\left[(h_4 - z)/(h_4 - h_3)\right]^k + \chi_c, & z \in [h_3, h_4] \\ \chi(z) = \chi_m\left[1 - e_o \cos(\pi z/(h_3 - h_2))\right], & z \in [h_2, h_3] \\ \chi(z) = (\chi_m - \chi_c)\left[(z - h_1)/(h_2 - h_1)\right]^k + \chi_c, & z \in [h_1, h_2] \end{cases} \tag{1}$$

where subscripts m and c denote the metal and ceramic constituents, respectively; k is the power-law index, which indicates the inhomogeneity of FGM ($k \geq 0$); e_o is the porosity coefficient, ($0 \leq e_o < 1$) [30].

b. FGM face-FG foam core-isotropic face (FGM-FS II)

For the second beam type, the top and bottom face layers are FGM and isotropic metal, respectively, while the core layer is a metal foam. The material properties of the layers vary as follows [24]

$$\begin{cases} \chi(z) = (\chi_m - \chi_c)\left[(h_4 - z)/(h_4 - h_3)\right]^k + \chi_c, & z \in [h_3, h_4] \\ \chi(z) = \chi_m\left[1 - e_o \cos\left(\pi z/(h_3 - h_2)\right)\right], & z \in [h_2, h_3] \\ \chi(z) = \chi_m, & z \in [h_1, h_2] \end{cases} \tag{2}$$

The meaning of the parameters in Eq. (2) is similar to those in Eq. (1).

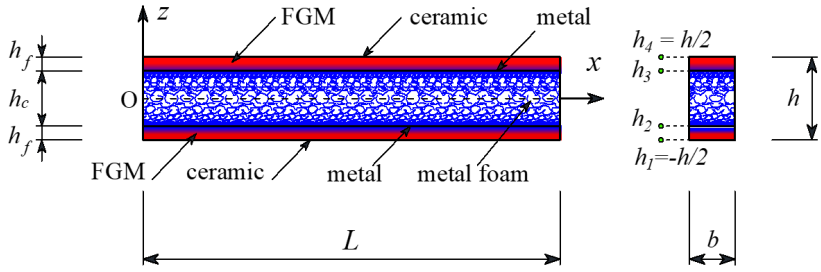

(a) FGM-FS I: FGM face-FG foam core-FGM face

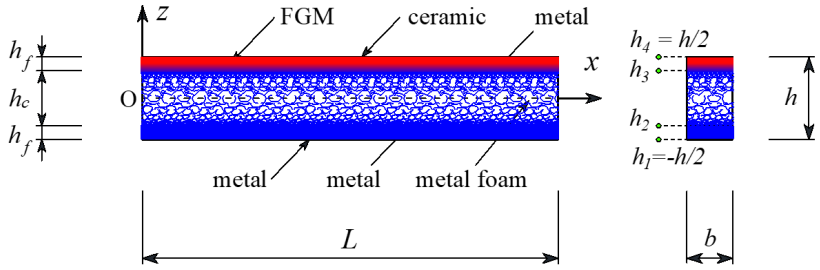

(b) FGM-FS II: FGM face-FG foam core-isotropic face

Figure 1. Configuration and geometry parameters of FGM-FS beams

It should be noted that various porosity distribution models have been proposed in the literature, such as uniform, symmetric, asymmetric distributions [24, 30]. Among them, symmetric cosine-based porosity distribution, in which the porosity is designed to be maximum at the mid-plane and to gradually decrease toward the top and bottom surfaces, has been reported to provide favorable structural performance from a mechanical perspective [24, 30]. In the present study, the foam core of the FGM-FS beams adopts this distribution due to its demonstrated advantages. Moreover, the adopted porosity distribution is combined with metal or FGM face layers, in which the metal constituent is in direct contact with the metal foam core. This configuration ensures a smooth and continuous variation of material properties across the thickness of the beams (see Eqs. (1) and (2)), thereby avoiding abrupt changes at the core-face interfaces. As a result, interfacial stress concentrations are significantly reduced, leading to a lower risk of delamination.

2.2. Thermal variations

In this study, three cases of temperature rise across the beam thickness are considered: uniform temperature rise (UTR), linear temperature rise (LTR), and nonlinear temperature rise (NTR) due to heat conduction. The beams are assumed in the stress-free state at the temperature of $T_0 = 300$ K.

a. Uniform temperature rise (UTR)

The current temperature T at any point in the beams increases by ΔT from the initial temperature T_0. It can be expressed as

$$T(z) = T_0 + \Delta T \tag{3}$$

b. Linear temperature rise (LTR)

The temperature varies linearly along the thickness of the beams as follows

$$T(z) = T_b + \Delta T\left(\frac{z}{h} + \frac{1}{2}\right); \quad (\Delta T = T_t - T_b) \tag{4}$$

where T_b and T_t are corresponding to the current temperatures at the bottom and top surfaces of the beams.

c. Nonlinear temperature rise (NTR)

In this case, the variation of temperature in the beams through the z-direction follows the steady-state Fourier heat conduction equation as

$$-\frac{d}{dz}\left(\kappa^{(i)}(T,z)\frac{dT(z)}{dz}\right) = 0 \tag{5}$$

Based on the thermal continuity conditions at the interfaces between the two adjacent layers, together with the boundary condition $T = T_b$ at the bottom surface and $T = T_t$ at the top surface, the solution of Eq. (5) yields [31]:

$$T^{(i)}(Z) = \Delta T\frac{\Xi^{(i)}}{\Gamma} + T_b; \quad \Delta T = (T_t - T_b) \tag{6}$$

where

$$\begin{cases} \Xi^{(1)} = \displaystyle\int_{h_1}^{z}\frac{1}{\kappa^{(1)}(z)}dz, & h_1 \le z \le h_2 \\ \Xi^{(2)} = \displaystyle\int_{h_1}^{h_2}\frac{1}{\kappa^{(1)}(z)}dz + \int_{h_2}^{z}\frac{1}{\kappa^{(2)}(z)}dz, & h_2 \le z \le h_3 \\ \Xi^{(3)} = \displaystyle\int_{h_1}^{h_2}\frac{1}{\kappa^{(1)}(z)}dz + \int_{h_2}^{h_3}\frac{1}{\kappa^{(2)}(z)}dz + \int_{h_3}^{z}\frac{1}{\kappa^{(3)}(z)}dz, & h_3 \le z \le h_4 \end{cases} \tag{7}$$

$$\Gamma = \int_{h_1}^{h_2}\frac{1}{\kappa^{(1)}(z)}dz + \int_{h_2}^{h_3}\frac{1}{\kappa^{(2)}(z)}dz + \int_{h_3}^{h_4}\frac{1}{\kappa^{(3)}(z)}dz \tag{8}$$

and $\kappa^{(i)}$, $i = 1, 2, 3$, indicates the thermal conductivity coefficient corresponding to the i-th layer.

For simplicity and to highlight the fundamental buckling mechanisms, the material properties are assumed to be temperature-independent in the present study. Although this assumption may influence the quantitative accuracy of critical buckling temperatures at high thermal loads, it allows for a clear assessment of the relative effects of beam theories and key parameters on the thermal buckling behavior.

2.3. The displacement and strain fields

A unified displacement field based on quasi-3D theory, in which both shear and normal deformations are taken into consideration, can be expressed as [4]

$$\mathbf{d} = \begin{Bmatrix} u(x) \\ w(x) \end{Bmatrix} = \boldsymbol{\theta}_1 \mathbf{B}_1 \tag{9}$$

where

$$\boldsymbol{\theta}_1 = \begin{bmatrix} 1 & 0 & -z & f(z) & 0 \\ 0 & 1 & 0 & 0 & \dfrac{\partial f(z)}{\partial z} \end{bmatrix} \tag{10}$$

$$\mathbf{B}_1^T = \left\{ u_o(x) \quad w_o(x) \quad \frac{\partial w_o(x)}{\partial x} \quad \beta_{os}(x) \quad w_{oz}(x) \right\} \tag{11}$$

In Eqs. (9) and (11), there are four unknown displacements on the mid-plane, i.e., u_o, w_o, β_{os}, and w_{oz}, to be determined. $f(z)$ is the shape function characterizing the shear strain and shear stress distributions over the beam's cross-section. There have been lots of shape functions proposed by authors. They were reviewed in detail by Sayyad and Ghugal [4]. Among them, Reddy's third-order function $f(z) = z - 4z^3/\left(3h^2\right)$ [32] is used extensively in the literature. This function is adopted to model the beams in the present study.

It is noted that Eqs. (9)-(11) are formulated within the quasi-3D framework; however, they can be simplified for use in the other beam theories through appropriate modifications of the functions $f(z)$ and w_{oz}. For instance, setting $f(z) = 0$ corresponds to CBT; $f(z) = z$ and $w_{oz} = 0$ corresponds to FBT; and $w_{oz} = 0$ corresponds to HOBT. It should be noted that HOBT, based on Reddy's third-order function, is also called the third-order beam theory (TBT).

The strain-displacement relationship can be expressed as follows

$$\boldsymbol{\varepsilon} = \begin{Bmatrix} \varepsilon_x \\ \varepsilon_z \\ \gamma_{xz} \end{Bmatrix} = \boldsymbol{\theta}_2 \mathbf{B}_2 \tag{12}$$

where

$$\boldsymbol{\theta}_2 = \begin{bmatrix} 1 & -z & f(z) & 0 & 0 & 0 \\ 0 & 0 & 0 & \dfrac{\partial^2 f(z)}{\partial z^2} & 0 & 0 \\ 0 & 0 & 0 & 0 & \dfrac{\partial f(z)}{\partial z} & \dfrac{\partial f(z)}{\partial z} \end{bmatrix} \tag{13}$$

$$\mathbf{B}_2^T = \left\{ \frac{\partial u_o}{\partial x} \quad \frac{\partial^2 w_o}{\partial x^2} \quad \frac{\partial \beta_{os}}{\partial x} \quad w_{oz} \quad \beta_{os} \quad \frac{\partial w_{oz}}{\partial x} \right\} \tag{14}$$

2.4. Hooke's law

The stress-strain relations in thermal environment based on the quasi-3D theory can be written as

$$\boldsymbol{\sigma} = \begin{Bmatrix} \sigma_x \\ \sigma_z \\ \tau_{xz} \end{Bmatrix} = \underbrace{\begin{bmatrix} C_{11} & C_{12} & 0 \\ C_{21} & C_{22} & 0 \\ 0 & 0 & C_{33} \end{bmatrix}}_{\mathbf{E}_d} \left(\underbrace{\begin{Bmatrix} \varepsilon_x \\ \varepsilon_z \\ \gamma_{xz} \end{Bmatrix}}_{\boldsymbol{\varepsilon}} - \underbrace{\begin{Bmatrix} \alpha\,(T-T_0) \\ \alpha\,(T-T_0) \\ 0 \end{Bmatrix}}_{\boldsymbol{\varepsilon}^{th}} \right) = \mathbf{E}_d \left(\boldsymbol{\varepsilon} - \boldsymbol{\varepsilon}^{th} \right) \tag{15}$$

where $C_{ij}\,(i, j = 1, 2, 3)$ are the stiffness coefficients defined in terms of the Young's modulus E and Poisson's ratio ν as

$$C_{11} = C_{22} = \frac{E}{1-\nu^2}; \quad C_{12} = C_{21} = \nu C_{11}; \quad C_{33} = G = \frac{E}{2+2\nu} \tag{16}$$

It is to be noted that Eq. (15) and the stiffness coefficients in Eq. (16) are expressed for the quasi-3D theory with the plane stress condition. The other beam theories can also use this relation by adjusting the coefficients. For example, setting $C_{11} = E$, $C_{12} = C_{21} = 0$ for CBT and TBT; setting $C_{11} = E$, $C_{12} = C_{21} = 0$ and $C_{33} = k_s G$ in which k_s is the shear correction factor, for FBT. This factor is assumed to have the constant with the classical value of $k_s = 5/6$ for the beams with rectangular cross-section. It is recognized that, for FGM, k_s may vary through the thickness due to material inhomogeneity. However, the constant value of 5/6 is adopted in the present study for consistency with conventional FBT formulations and to maintain analytical simplicity, which could be acceptable for the investigation of the global buckling behavior of FGM-FS beams.

2.5. Energy expressions of the beams

Neglecting the thermal strains ε^{th}, the internal strain energy of the beams due to the mechanical strains ε is calculated as the following expression

$$U^{in} = \frac{1}{2}\int_V \boldsymbol{\sigma}^T \boldsymbol{\varepsilon} dV = \frac{1}{2}\int_V \boldsymbol{\varepsilon}^T \mathbf{E}_d \boldsymbol{\varepsilon} dV \tag{17}$$

Substituting Eq. (12) into Eq. (17), the strain energy can be expressed through the displacements

$$U^{in} = \frac{1}{2}\int_0^L \mathbf{B}_2^T \mathbf{D}_E \mathbf{B}_2 dx \tag{18}$$

in which $\mathbf{D}_E$ is the 6×6 square matrix of stiffnesses given by

$$\mathbf{D}_{E(6\times6)} = \int_A \boldsymbol{\theta}_2^T \mathbf{E}_d \boldsymbol{\theta}_2 dA \tag{19}$$

The potential energy of the mechanical and thermal loads can be expressed as

$$U^e = \frac{1}{2}\int_0^L P^l \left(\frac{\partial w_o(x)}{\partial x} \right)^2 dx + \frac{1}{2}\int_0^L N^{th} \left(\frac{\partial w_o(x)}{\partial x} \right)^2 dx \tag{20}$$

where P^l are the mechanical loads acting axially at the two ends of the beams; N^{th} is the thermal stress resultant determined by on the quasi-3D theory as

$$N^{th} = -b\int_{h_1}^{h_4}(C_{11}+C_{12})\alpha\,(T-T_0)\,dz = b\int_{h_1}^{h_4}\left(\sigma_{x1}^{th}+\sigma_{x2}^{th}\right)dz \tag{21}$$

$$\sigma_{x1}^{th} = -C_{11}\alpha\,(T-T_0)\,;\sigma_{x2}^{th} = -C_{12}\alpha\,(T-T_0) \tag{22}$$

where $\sigma_{x1}^{th}, \sigma_{x2}^{th}$ are axial stresses due to the thermal strains in x-and z-directions, respectively.

In the case when the axial stresses due to thermal strains in the z-direction (the thickness) are not considered, as in the study of Nguyen et al. [16], by neglecting σ_{x2}^{th} (setting $\sigma_{x2}^{th} = 0$), the thermal stress resultant reduces to:

$$N^{th} = b\int_{h_1}^{h_4}\sigma_{x1}^{th}dz \tag{23}$$

In the case of the other beam theories, i.e., CBT, FBT and TBT, (setting $C_{11} = E$, $C_{12} = 0$), Eq. (21) is reduced to:

$$N^{th} = -b\int_{h_1}^{h_4}C_{11}\alpha\,(T-T_0)\,dz = -b\int_{h_1}^{h_4}E\alpha\,(T-T_0)\,dz \tag{24}$$

In the above equations, the volume, cross-section area, and length of the beams are abbreviated as V, A, and L, respectively.

2.6. Ritz method-based solution

In the present study, the Ritz method is employed to discretize the governing equations into an algebraic equation system. According to the concept of the method, the displacement fields u_o, w_o, β_o, and w_{oz} are approximated by the following series:

$$u_o = \sum_{i=1}^{N}U_o^{(i)}\varphi_{uo}^{(i)},\ w_o = \sum_{i=1}^{N}W_o^{(i)}\varphi_{wo}^{(i)},\ \beta_o = \sum_{i=1}^{N}\Phi_{os}^{(i)}\varphi_{so}^{(i)},\ w_{oz} = \sum_{i=1}^{N}W_{oz}^{(i)}\varphi_{woz}^{(i)} \tag{25}$$

where $U_o^{(i)}$, $W_o^{(i)}$, $\Phi_{os}^{(i)}$, and $W_{oz}^{(i)}$ are the unknown coefficients, $\varphi_{uo}^{(i)}$, $\varphi_{wo}^{(i)}, \varphi_{so}^{(i)}$, and $\varphi_{woz}^{(i)}$ are admissible functions for the field variables u_o, w_o, β_o and w_{oz}, respectively. In this study, trigonometric functions that satisfy the specified essential boundary conditions are selected for the admissible functions. These functions for simply-supported (SS) and clamped-clamped (CC) beams with axially movable/immovable edges are stated in Table 1. The kinematic boundary conditions are given in Table 2 [33]. N is the total number of terms in the series and is determined by the convergence test in the analysis for satisfactory accuracy. N is the same for different approximated functions in the analysis for convenience.

Substituting the displacement forms of Eq. (25) into the energy expressions, Eqs. (18) and (20), to express them in terms of the unknown coefficients, and then applying the principle of the minimum potential energy by taking the derivative of total energy ($U^{in} + U^e$) with respect to the coefficients as.

$$\begin{cases}\dfrac{\partial\,(U^{in}+U^e)}{\partial U_o^{(i)}} = 0, & \dfrac{\partial\,(U^{in}+U^e)}{\partial W_o^{(i)}} = 0,\\ \dfrac{\partial\,(U^{in}+U^e)}{\partial \Phi_{os}^{(i)}} = 0, & \dfrac{\partial\,(U^{in}+U^e)}{\partial W_{oz}^{(i)}} = 0, \quad i = 1,...,N\end{cases} \tag{26}$$

Table 1. Trigonometric admissible functions [33]

Boundary conditions	$\varphi_{uo}^{(i)}$	$\varphi_{wo}^{(i)}$	$\varphi_{so}^{(i)}$	$\varphi_{woz}^{(i)}$
SS$^{(I)}$	$1-\cos\left((2i-1)\pi x/L\right)$	$\sin\left((2i-1)\pi x/L\right)$	$\cos\left((2i-1)\pi x/L\right)$	$\sin\left((2i-1)\pi x/L\right)$
SS$^{(II)}$	$\sin\left(i\pi x/L\right)$	$\sin\left((2i-1)\pi x/L\right)$	$\cos\left((2i-1)\pi x/L\right)$	$\sin\left((2i-1)\pi x/L\right)$
CC$^{(I)}$	$1-\cos\left((2i-1)\pi x/L\right)$	$1-\cos\left(2i\pi x/L\right)$	$\sin\left(i\pi x/L\right)$	$1-\cos\left(2i\pi x/L\right)$
CC$^{(II)}$	$\sin\left(i\pi x/L\right)$	$1-\cos\left(2i\pi x/L\right)$	$\sin\left(i\pi x/L\right)$	$1-\cos\left(2i\pi x/L\right)$

$^{(I)}$ axially movable edges; $^{(II)}$ axially immovable edges.

This procedure yields the simultaneous algebraic equations which are presented in the matrix form as

$$\left([\mathbf{K}]_{4N\times 4N} + P^l\left[\mathbf{K}_G\right]_{4N\times 4N} + N^{th}\left[\mathbf{K}_G\right]_{4N\times 4N}\right)\begin{Bmatrix}\mathbf{U}_o\\ \mathbf{W}_o\\ \mathbf{\Phi}_{os}\\ \mathbf{W}_{oz}\end{Bmatrix}_{4N\times 1} = \{\mathbf{0}\} \tag{27}$$

where $[\mathbf{K}]$ and $[\mathbf{K}_G]$ are the elastic and geometric stiffness matrices, respectively.

The more explicit vectors of unknown coefficients of the admissible functions are described as

$$\begin{cases}\mathbf{U}_o = \left\{U_o^{(1)} \quad U_o^{(2)} \quad ... \quad U_o^{(N)}\right\}^T\\ \mathbf{W}_o = \left\{W_o^{(1)} \quad W_o^{(2)} \quad ... \quad W_o^{(N)}\right\}^T\\ \mathbf{\Phi}_{os} = \left\{\Phi_{os}^{(1)} \quad \Phi_{os}^{(2)} \quad ... \quad \Phi_{os}^{(N)}\right\}^T\\ \mathbf{W}_{oz} = \left\{W_{oz}^{(1)} \quad W_{oz}^{(2)} \quad ... \quad W_{oz}^{(N)}\right\}^T\end{cases} \tag{28}$$

Table 2. Kinematic boundary conditions

Boundary conditions	Left edge ($x=0$)	Right edge ($x=L$)
SS$^{(I)}$	$u_o=0,\ w_o=0,\ w_{oz}=0$	$w_o=0,\ w_{oz}=0$
SS$^{(II)}$	$u_o=0,\ w_o=0,\ w_{oz}=0$	$u_o=0,\ w_o=0,\ w_{oz}=0$
CC$^{(I)}$	$u_o=0,\ w_o=0,\ \partial w_o/\partial x=0,$ $\beta_o=0,\ w_{oz}=0,\ \partial w_{oz}/\partial x=0$	$w_o=0,\ \partial w_o/\partial x=0,$ $\beta_o=0,\ w_{oz}=0,\ \partial w_{oz}/\partial x=0$
CC$^{(II)}$	$u_o=0,\ w_o=0,\ \partial w_o/\partial x=0,$ $\beta_o=0,\ w_{oz}=0,\ \partial w_{oz}/\partial x=0$	$u_o=0,\ w_o=0,\ \partial w_o/\partial x=0,$ $\beta_o=0,\ w_{oz}=0,\ \partial w_{oz}/\partial x=0$

In this study, the thermal buckling and mechanical buckling problems are considered separately, without coupling. The coupling effect is devoted to future research. To this end, in Eq. (27), setting either $N^{th}=0$ or $P^l=0$, the problem is reduced to the mechanical or thermal buckling analysis, respectively.

By setting the determinant of the coefficient matrix in Eq. (27) to be zero results in the eigenvalues, and then determines the critical buckling load P_{cr}^l/the critical buckling temperature ΔT_{cr}. Note that ΔT_{cr} is $T-T_0$ (for UTR) or T_t-T_b (for LTR and NTR) that makes the beams buckle.

3. Numerical examples and discussion

Through this section, the mechanical/thermal buckling of FGM-FS beams is numerically studied. Original material properties are as: metal is Aluminum (Al) $E_m=70$ GPa, $\nu_m=0.3$, $\alpha_m=23\times$

10^{-6}/K, $\kappa_m = 204$ W/mK; ceramic is Alumina (Al_2O_3) $E_c = 380$ GPa, $\nu_c = 0.3$, $\alpha_c = 7.4 \times 10^{-6}$/K, $\kappa_c = 10.4$ W/mK (referred from Yaghoobi and Fereidoon [34], Kiani and Eslami [12], Zenkour and Sobhy [35], Zenkour and Radwan [36]). It is assumed that the temperature at the bottom surface of the beams is $T_b = T_0 = 300$ K for LTR and NTR.

As mentioned above, two types of boundary condition (BC), i.e., SS and CC, with/without axially movable end supports, are supposed to satisfy the condition of loads acting on the beams. Axially movable end supports ($SS^{(I)}$, $CC^{(I)}$) are imposed for the case of mechanical load, whereas axially immovable end supports ($SS^{(II)}$, $CC^{(II)}$) are for the thermal loads. Their kinematic conditions are given in Table 2. It should be noted that for FGM beams, the studies by Wang et al. [37] and by Trinh et al. [38] show that move/immovable end supports have significant effects on the predicted behavior of the FGM beams.

For convenience, the dimensionless forms of the mechanical buckling load are defined as

$$\hat{P}_{cr} = P^{l}_{cr}\frac{12L^2}{E_m b h^3} \tag{29}$$

where P^{l}_{cr} is the critical buckling load.

3.1. Convergence study and validation

The convergence study is performed by increasing the number of terms in the series expansion. The CC beams with parameters $k = 0.5$, $e_o = 0.5$, $h_c/h_f = 8$ are considered. The obtained results are presented in Table 3 for the mechanical buckling analysis and Table 4 for the thermal buckling analysis. It is seen from Tables 3 and 4 that (i) increasing the number of terms improves the accuracy of the results; (ii) the quasi-3D exhibits the lowest convergence rate, whereas the results obtained using the CBT, FBT, and TBT models converge to the exact solution (with four digits after the decimal) within two terms of the series ($N = 2$). In general, $N = 10$ terms are sufficient to achieve the satisfactory accuracy. Therefore, this value is used in the subsequent analyses.

Table 3. Convergence study for the critical buckling load $\hat{P}_{cr}$ of FGM-FS I beam ($L/h = 5$, $e_o = 0.5$, $h_c/h_f = 8$, $k = 0.5$, $CC^{(I)}$ boundary condition)

Theory	Number of terms N						
	1	2	4	6	8	10	12
CBT	66.7925	66.7925	66.7925	66.7925	66.7925	66.7925	66.7925
FBT	66.7925	40.0543	40.0543	40.0543	40.0543	40.0543	40.0543
TBT	66.7925	34.2630	34.2630	34.2630	34.2630	34.2630	34.2630
quasi-3D	71.2115	35.6757	35.5981	35.5689	35.5534	35.5437	35.5373

After examining the convergence and finding out the appropriate terms of the admissible functions for the analysis, several numerical examples are conducted, and their results are compared with other authors to validate the current study. First, an FGM sandwich beam with a solid hard core is considered by interchanging the role of ceramic (χ_c) and metal (χ_m) in the formulations of Eq. (1), and by setting $e_o = 0$. The mechanical buckling of this beam was previously investigated by Vo et al. [5] based on TBT and FEM, and by Vo et al. [10] based on quasi-3D theory and FEM. The data presented in Table 5 are in excellent agreement with the results reported by Vo et al. [5] and Vo et al. [10].

Another validation example concerns the mechanical buckling of a single layer foam beam, which is obtained by setting $h_f = 0$ (i.e., neglecting the faces) in the analysis. This problem was conducted

Table 4. Convergence study for the critical buckling temperature ΔT_{cr} (in K) of FGM-FS II beam ($L/h = 20$, $e_o = 0.5$, $h_c/h_f = 8$, $k = 0.5$, LTR, CC$^{(II)}$ boundary condition)

Theory	Number of terms N						
	1	2	4	6	8	10	12
CBT	1264.421	1201.485	1201.485	1201.485	1201.485	1201.485	1201.485
FBT	1264.421	1160.308	1160.308	1160.308	1160.308	1160.308	1160.308
TBT	1264.421	1148.481	1148.481	1148.481	1148.481	1148.481	1148.481
quasi-3D	943.469	837.721	825.896	821.523	819.258	817.882	816.963

Table 5. Comparison of the critical buckling load $\hat{P}_{cr}$ of FGM-FS I beam ($L/h = 5$, $e_o = 0$, $h_c/h_f = 8$)

BC	k	TBT		quasi-3D	
		Present	[5]	Present	[10]
SS$^{(I)}$	0.5	41.9897	41.9897	42.8751	42.8751
	5	32.7725	32.7725	33.4957	33.4958
CC$^{(I)}$	0.5	134.2865	134.2870	141.9065	141.7880
	5	108.2967	108.2970	114.8656	114.7700

Table 6. Comparison of the critical buckling load P^l_{cr} (in N) of single layer porous beam ($e_o = 0.99$)

Theory	Source	L/h		
		20	25	50
CBT	Present	27 054	17 315	4329
	Tang et al. [39]	27 054	17 315	4329
FBT	Present	26 756	17 192	4321
	Kitipornchai et al. [40]	26 756	17 192	4321

by Tang et al. [39], and Kitipornchai et al. [40] using the parameters $E_m = 205$ GPa, $\nu = 0.3$, $h = 0.1$ m, and $b = 0.001$ m. SS$^{(I)}$ beam with three cases of span-to-height ratio (L/h) are considered. The results in Table 6 show that the critical buckling load obtained in the present study is identical to that reported by the aforementioned authors.

The third comparison study concerns the thermal buckling of single FGM beams without porosities which is modelled by setting the thickness of the core and bottom layers to zero. The thermal bucking of these beams was studied by Kiani and Eslami [12] using CBT and analytical solution, and by Esfahani et al. [13] using FBT and generalized differential quadrature method (GDQM). For consistency and comparison, the material composition of the FGM, the mechanical properties, and the working conditions are adopted from Refs. [12, 13].

The numerical results are reported in Tables 7 and 8. The comparisons show that the present results agree very well with those of Kiani and Eslami [12] and Esfahani et al. [13]. In addition, as expected, a significant difference is observed between SS$^{(I)}$ and SS$^{(II)}$ cases in Table 7 when $k \neq 0$, confirming that axially movable/immovable end support has a strong effect on the computed results. Thus, it is necessary to carefully take into consideration the types of BC in the analysis of FGM beams.

Table 7. Comparison of the critical buckling temperature ΔT_{cr} (in K) of single layer Al_2O_3/Al FGM beam (SS, CBT, LTR)

L/h	BC	Source	$k = 0$	0.5	1	2	5	10
10	$SS^{(I)}$	This study	2212.88	1249.79	959.01	797.03	804.31	851.48
	$SS^{(II)}$	This study	2212.88	1325.55	1101.59	990.09	973.01	951.98
	$SS^{(I)}$	Ref. [12]	2212.88	1249.79	959.01	797.03	804.31	851.48
30	$SS^{(I)}$	This study	236.99	129.97	98.22	80.73	81.72	86.73
	$SS^{(II)}$	This study	236.99	138.39	114.06	102.19	100.46	97.90
	$SS^{(I)}$	Ref. [12]	236.99	129.97	98.22	80.73	81.72	86.73

Table 8. Comparison of the critical buckling temperature ΔT_{cr} (in K) of single layer SUS_{304}/Si_3N_4 FGM beam (FBT)

Temperature distribution	L/h	BC	Source	$k = 0$	0.5	1	2	5	10
UTR	25	$SS^{(I)}$	This study	175.33	129.02	116.08	107.22	99.89	95.27
		$SS^{(I)}$	Ref. [13]	175.32	129.02	116.07	107.21	99.88	95.26
		$CC^{(II)}$	This study	692.81	509.99	458.77	423.62	394.49	376.22
		$CC^{(II)}$	Ref. [13]	692.70	509.89	458.68	423.53	394.39	376.14
NTR	40	$SS^{(I)}$	This study	127.32	98.12	87.42	78.95	71.00	66.16
		$SS^{(I)}$	Ref. [13]	127.32	97.97	87.23	78.74	70.77	65.92
		$CC^{(II)}$	This study	536.64	422.79	380.23	346.10	313.59	293.84
		$CC^{(II)}$	Ref. [13]	536.62	422.18	379.47	345.22	312.64	292.87

3.2. Parametric studies

a. Mechanical buckling investigations

Tables 9 and 10 list the dimensionless critical buckling load calculated with the different values of power-law index k for two cases of span-to-heigh ratio ($L/h = 5$ and $L/h = 20$). Two sandwich beam types (FGM-FS I and FGM-FS II), as well as two BCs ($CC^{(I)}$ and $SS^{(I)}$), are considered. Observing the numerical results in the tables shows that different beam theories exhibit importantly deviate values of the critical buckling load; this effect is stronger for the thick beams ($L/h = 5$) than the thin ones ($L/h = 20$), or for $CC^{(I)}$ beams than $SS^{(I)}$ ones, or FGM-FS I beam than FGM-FS II one. Additionally, FGM-FS I beam with symmetric layer structure has a greater critical buckling load than FGM-FS II one, as expected. Also, as k increases, the critical buckling load increases. This is because of the fact that the higher value of k leads to a higher density of the ceramic constituent, which has a higher elastic modulus, thus makes the beams stiffer. From an application standpoint, tailoring the material gradation through k provides a practical design parameter to enhance buckling performance of the FGM-FS beams.

Numerical results in Tables 9 and 10 also show that among the three shear deformation theories considered, the critical buckling load predicted by FBT is distinctly different from that predicted by TBT/quasi-3D theory. For example, the relative difference is $\left(\hat{P}_{cr}|_{\text{FBT}} - \hat{P}_{cr}|_{\text{TBT}}\right)/\hat{P}_{cr}|_{\text{TBT}} \times 100\% = (64.851 - 46.123)/46.123 \times 100\% = 40.61\%$ for FGM-FS I beam, is $(39.694 - 32.928)/32.928 \times 100\% = 20.55\%$ for FGM-FS II one (the data are taken from Tables 9 and 10 with $k = 10$, $L/h = 5$, $CC^{(I)}$). Furthermore, it is interesting in Table 10 that the FGM-FS II beam with $L/h = 20$ and $SS^{(I)}$, the quasi-3D gives slightly higher critical buckling load than CBT does when $k > 2$. The reason is

that the thickness stretching effect included in the quasi-3D theory may make the beam slightly stiffer. This reason also explains why the critical buckling load of the quasi-3D theory is a little greater than that of TBT in the tables.

Table 9. The critical buckling load $\hat{P}_{cr}$ of FGM-FS I beam ($e_o = 0.5$, $h_c/h_f = 8$)

BC	k	$L/h = 5$				$L/h = 20$			
		CBT	FBT	TBT	quasi-3D	CBT	FBT	TBT	quasi-3D
SS$^{(I)}$	0	8.955	7.960	7.820	7.972	8.955	8.886	8.874	8.887
	0.5	16.698	14.310	13.475	13.705	16.698	16.525	16.451	16.474
	1	20.407	17.314	15.897	16.157	20.407	20.181	20.050	20.077
	2	23.956	20.190	18.079	18.365	23.956	23.680	23.478	23.509
	5	27.281	22.901	20.041	20.350	27.281	26.959	26.677	26.713
	10	28.694	24.063	20.868	21.186	28.694	28.353	28.035	28.073
CC$^{(I)}$	0	35.822	23.884	22.707	23.793	35.822	34.736	34.566	35.052
	0.5	66.792	40.054	34.263	35.543	66.792	64.117	63.018	63.852
	1	81.628	47.611	38.400	39.709	81.628	78.139	76.213	77.205
	2	95.824	54.881	41.848	43.168	95.824	91.555	88.610	89.747
	5	109.127	61.826	44.840	46.171	109.127	104.147	100.071	101.343
	10	114.778	64.851	46.123	47.462	114.778	109.509	104.921	106.250

Table 10. The critical buckling load $\hat{P}_{cr}$ of FGM-FS II beam ($e_o = 0.5$, $h_c/h_f = 8$)

BC	k	$L/h = 5$				$L/h = 20$			
		CBT	FBT	TBT	quasi-3D	CBT	FBT	TBT	quasi-3D
SS$^{(I)}$	0	8.955	7.960	7.820	7.972	8.955	8.886	8.874	8.887
	0.5	12.188	10.673	10.291	10.510	12.188	12.081	12.049	12.119
	1	13.373	11.691	11.157	11.417	13.373	13.254	13.208	13.331
	2	14.333	12.537	11.847	12.148	14.333	14.206	14.147	14.329
	5	15.093	13.230	12.392	12.733	15.093	14.962	14.890	15.132
	10	15.375	13.495	12.597	12.955	15.375	15.243	15.166	15.434
CC$^{(I)}$	0	35.822	23.884	22.707	23.793	35.822	34.736	34.566	35.052
	0.5	48.853	31.137	28.175	29.396	48.853	47.176	46.694	47.498
	1	53.691	34.034	29.967	31.234	53.691	51.821	51.140	52.158
	2	57.646	36.574	31.368	32.673	57.646	55.643	54.755	55.999
	5	60.805	38.792	32.486	33.827	60.805	58.722	57.638	59.104
	10	61.986	39.694	32.928	34.285	61.986	59.884	58.720	60.282

Fig. 2 examines the effects of the porosity coefficient e_o in coupling with different beam theories on the critical buckling load of the sandwich beams. As can be seen, an increase of e_o results in a reduction of the critical buckling load for all beam theories. This is because an increase in the porosity coefficient leads to a reduction of effective moduli (E and G), making the beams more flexible. It is also noted that the rate of decrease in the critical buckling load predicted by TBT/quasi-3D is faster than that predicted by CBT/FBT.

Fig. 3 depicts the variation of the critical buckling load with respect to the layer thickness ratio h_c/h_f. When h_c/h_f increases, the soft core becomes thicker, whereas the hard skins become thinner;

thus, the sandwich beams are more flexible and the critical buckling load decreases for all beam models. Also, it is observed that the decreased rate of FGM-FS I beam is faster than that of FGM-FS II one.

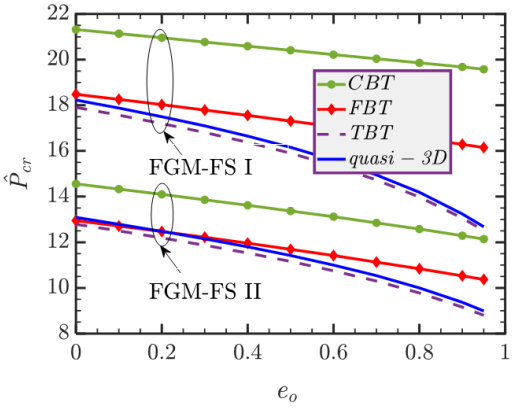

Figure 2. The critical buckling load $\hat{P}_{cr}$ of the sandwich beams with respect to e_o ($h_c/h_f = 8$, $k = 1$, $L/h = 5$, SS$^{(\mathrm{I})}$)

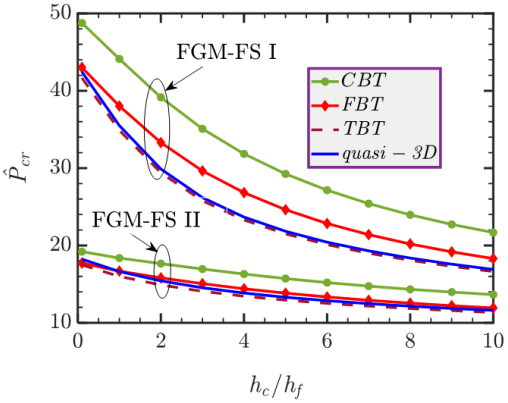

Figure 3. The critical bucking load $\hat{P}_{cr}$ of the sandwich beams with respect to h_c/h_f ($e_o = 0.5$, $k = 2$, $L/h = 5$, SS$^{(\mathrm{I})}$)

Overall, the mechanical buckling response results from the combined influence of the power-law index (k), porosity coefficient (e_o), layer thickness ratio (h_c/h_f), beam theories, and span-to-height ratio together with the kinematic assumptions of the adopted beam theory. Increasing k enhances the stiffness and improves stability, whereas higher porosity and larger core thickness generally reduce the critical load due to stiffness degradation. These interactions are more pronounced for thick beams, where shear effects are significant and refined theories (TBT or quasi-3D) provide more reliable predictions. From a design standpoint, higher k values with moderate porosity and controlled core thickness offer an effective way to enhance mechanical buckling resistance while maintaining the lightweight characteristic.

b. Thermal buckling investigations

This section investigates the buckling response of the sandwich beams subjected to thermal loads. Tables 11–13 present the critical buckling temperature of FGM-FS I and FGM-FS II beams predicted by the different beam models. Three types of temperature distribution (UTR, LTR, and NTR), along with various values of power-law index k and two span-to-height ratios ($L/h = 5$ and $L/h = 20$) are considered. It should be noted that in the quasi-3D* model, the axial stress σ^{th}_{x2} (see Eq. (21)) induced by the thermal strains in the thickness direction is not included in the analysis (setting $\sigma^{th}_{x2} = 0$).

The obtained results in Tables 11–13 show that thick beams ($L/h = 5$) exhibit significantly higher critical buckling temperature than thin beams, as expected. The critical buckling temperature under UTR is smaller than that under LTR/NTR since the whole beam is uniformly heated by ΔT, while in LTR/NTR, the temperature gradient ranges from zero at the bottom to ΔT at the top.

For thick beams, the results predicted by the four beam theories differ noticeably. It is worth noting that, unlike the mechanical buckling results discussed earlier, the quasi-3D predictions are significantly smaller than those of other beam models (CBT, FBT, TBT). This behavior is attributed to the additional compressive axial stress σ^{th}_{x2} (see Eq. (21)) induced by the thickness-direction thermal strain, which is explicitly accounted for in the quasi-3D theory. This thermally induced axial stress reduces the geometrical stiffness and has a destabilizing effect on the thermal buckling response. Furthermore, the results obtained from the quasi-3D* theory are higher than those of the quasi-3D

theory but slightly lower than those predicted by TBT, as expected, since the quasi-3D* formulation does not include the axial stress σ_{x2}^{th} induced by the thermal strains in the thickness direction.

Table 11. The critical buckling temperature $\Delta T_{cr} \times 10^{-3}$ (in K) of the sandwich beams ($e_o = 0.5$, $h_c/h_f = 8$, UTR, CC$^{(II)}$)

k	$L/h = 5$					$L/h = 20$				
	CBT	FBT	TBT	quasi-3D	quasi-3D*	CBT	FBT	TBT	quasi-3D	quasi-3D*
FGM-FS I										
0	8.788	5.859	5.571	4.084	5.313	0.549	0.532	0.530	0.375	0.489
1	15.454	9.014	7.270	5.260	6.842	0.965	0.924	0.901	0.638	0.831
2	18.027	10.325	7.873	5.683	7.391	1.126	1.076	1.041	0.737	0.960
5	20.792	11.779	8.543	6.156	8.006	1.299	1.240	1.191	0.843	1.098
10	22.107	12.490	8.883	6.397	8.319	1.381	1.318	1.263	0.894	1.163
FGM-FS II										
0	8.788	5.859	5.571	4.084	5.313	0.549	0.532	0.530	0.375	0.489
1	11.432	7.256	6.390	4.660	6.060	0.714	0.689	0.680	0.485	0.631
2	12.210	7.762	6.658	4.853	6.311	0.763	0.736	0.725	0.518	0.675
5	12.950	8.283	6.939	5.056	6.575	0.809	0.781	0.767	0.550	0.716
10	13.272	8.523	7.074	5.154	6.703	0.829	0.801	0.786	0.564	0.734

Table 12. The critical buckling temperature $\Delta T_{cr} \times 10^{-3}$ (in K) of the sandwich beams ($e_o = 0.5$, $h_c/h_f = 8$, LTR, CC$^{(II)}$)

k	$L/h = 5$					$L/h = 20$				
	CBT	FBT	TBT	quasi-3D	quasi-3D*	CBT	FBT	TBT	quasi-3D	quasi-3D*
FGM-FS I										
0	17.577	11.719	11.142	8.169	10.624	1.098	1.065	1.060	0.751	0.978
1	30.908	18.028	14.540	10.521	13.682	1.931	1.849	1.803	1.277	1.662
2	36.055	20.649	15.746	11.366	14.780	2.253	2.153	2.083	1.475	1.920
5	41.584	23.559	17.086	12.312	16.010	2.599	2.480	2.383	1.687	2.196
10	44.214	24.981	17.767	12.794	16.637	2.763	2.636	2.526	1.788	2.327
FGM-FS II										
0	17.577	11.719	11.142	8.169	10.624	1.098	1.065	1.060	0.751	0.978
1	20.455	12.984	11.433	8.338	10.843	1.278	1.234	1.217	0.868	1.130
2	21.820	13.871	11.899	8.673	11.279	1.363	1.316	1.295	0.926	1.206
5	23.279	14.889	12.474	9.089	11.820	1.455	1.405	1.379	0.989	1.288
10	23.962	15.388	12.771	9.306	12.101	1.497	1.447	1.419	1.019	1.326

Interestingly, the outcomes of LTR and NTR are identical for the FGM-FS I beam with a symmetric configuration. Therefore, for the FGM-FS I beam, the LTR approach can be used as an alternative to NTR, reducing computational cost without sacrificing accuracy. In addition, the effect of the power-law index k on the thermal buckling of the beams is similar to that observed in the mechanical buckling case (as k increases, the critical buckling temperature increases).

Table 13. The critical buckling temperature $\Delta T_{cr} \times 10^{-3}$ (in K) of the sandwich beams ($e_o = 0.5$, $h_c/h_f = 8$, NTR, CC$^{(II)}$)

k	$L/h = 5$					$L/h = 20$				
	CBT	FBT	TBT	quasi-3D	quasi-3D*	CBT	FBT	TBT	quasi-3D	quasi-3D*
FGM-FS I										
0	17.575	11.718	11.141	8.168	10.623	1.098	1.065	1.060	0.751	0.978
1	30.906	18.027	14.539	10.521	13.681	1.931	1.849	1.803	1.277	1.662
2	36.053	20.648	15.745	11.365	14.780	2.253	2.152	2.083	1.475	1.920
5	41.583	23.559	17.086	12.312	16.010	2.599	2.480	2.383	1.687	2.196
10	44.215	24.982	17.768	12.795	16.638	2.763	2.636	2.526	1.788	2.327
FGM-FS II										
0	17.575	11.718	11.141	8.168	10.623	1.098	1.065	1.060	0.751	0.978
1	23.125	14.678	12.925	9.426	12.258	1.445	1.395	1.376	0.982	1.278
2	28.475	18.102	15.528	11.318	14.719	1.779	1.718	1.690	1.209	1.574
5	36.316	23.228	19.460	14.180	18.440	2.269	2.192	2.152	1.544	2.009
10	40.015	25.697	21.327	15.540	20.209	2.501	2.416	2.370	1.702	2.215

In Figs. 4 and 5, the effect of the porosity coefficient e_o is investigated for various beam theories and temperature rises. In general, in contrast to the mechanical buckling response, the critical buckling temperature can increase as e_o increases. This confirms the effectiveness of porous structures working in the thermal environment. More specifically, for FGM-FS I, the critical buckling temperature increases with CBT and FBT models, but increases initially and then decreases with TBT, quasi-3D and quasi-3D* models. However, for FGM-FS II, the critical buckling temperature increases initially and then decreases with respect to e_o for all beam models.

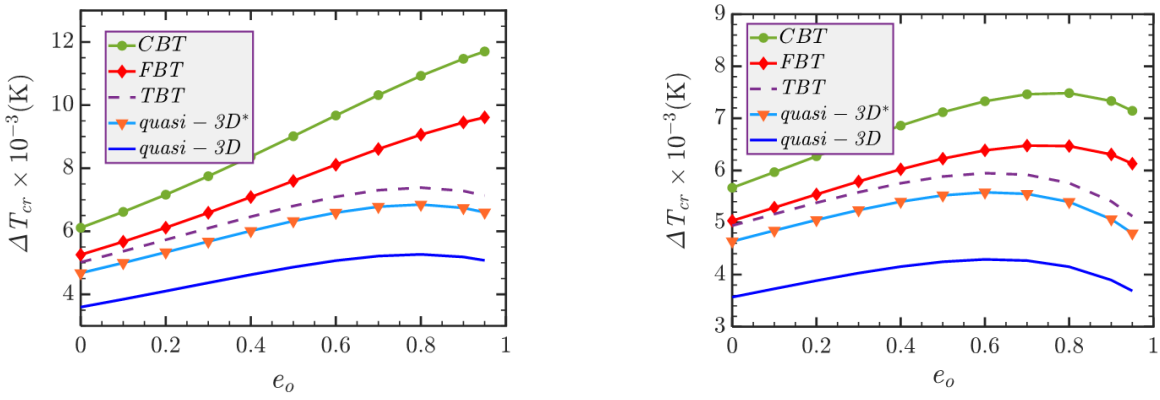

(a) FGM-FS I (b) FGM-FS II

Figure 4. The critical buckling temperature $\Delta T_{cr} \times 10^{-3}$ (in K) of the sandwich beams with respect to e_o for different beam models (NTR, $L/h = 10$, $k = 2$, $h_c/h_f = 8$, CC$^{(II)}$)

Figs. 6 and 7 illustrate the significant effect of layer thickness ratio h_c/h_f, associated with the beam theories and temperature rises, on the thermal buckling behavior of the beams. The most notable finding is that the critical buckling temperature may increase/increase initially and then decrease slightly/decrease then increase slightly as h_c/h_f increases (i.e., the soft core becomes thicker). This

trend is quite complex and depends on the type of sandwich beam (FGM-FS I or FGM-FS II) as well as the type of temperature rise. This finding underscores that there is no universally optimal core thickness, and thermal buckling design must be tailored to the specific operating conditions and sandwich configuration.

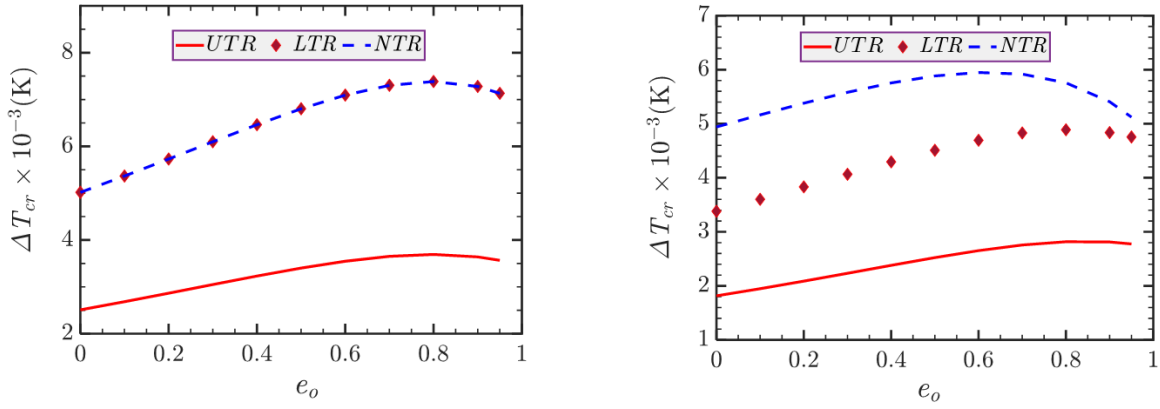

(a) FGM-FS I (b) FGM-FS II

Figure 5. The critical buckling temperature $\Delta T_{cr} \times 10^{-3}$ (in K) of the sandwich beams with respect to e_o for different temperature distributions (TBT, $L/h = 10$, $k = 2$, $h_c/h_f = 8$, CC$^{(II)}$)

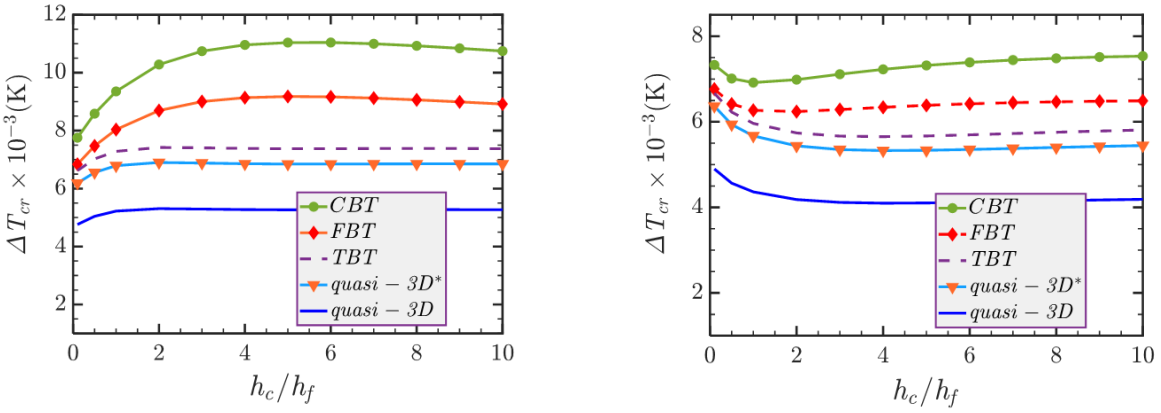

(a) FGM-FS I (b) FGM-FS II

Figure 6. The critical buckling temperature $\Delta T_{cr} \times 10^{-3}$ (in K) of the sandwich beams with respect to h_c/h_f for different beam models (NTR, $L/h = 10$, $k = 2$, $e_o = 0.8$, CC$^{(II)}$)

Finally, Figs. 5 and 7 show that the buckling temperature under NTR is higher than that under LTR for the FGM-FS II beam; however, they are identical for the FGM-FS I beam. Furthermore, in Figs. 4 and 6, the buckling temperature predicted by CBT is the highest, followed by FBT, TBT, quasi-3D* and quasi-3D models, respectively. The ranking of beam theories further demonstrates that CBT tend to overestimate thermal buckling resistance, while TBT and quasi-3D theories provide more conservative and realistic predictions. This reinforces the necessity of advanced modeling approaches in the thermal design of functionally graded sandwich beams.

Unlike the mechanical case, the thermal buckling is governed by the interaction between stiffness variation and thermally induced axial forces, especially when the thickness stretching effects are

considered. Although increasing k generally improves thermal stability, the effects of e_o and h_c/h_f may become non-monotonic depending on the sandwich configuration and temperature distribution. Therefore, thermal stability design requires balancing material gradation and geometric proportions under the appropriate TBT and quasi-3D theories, since CBT may overestimate the critical temperature. These results highlight the necessity of selecting both structural parameters and beam theory consistently for thermal buckling of FGM-FS beams.

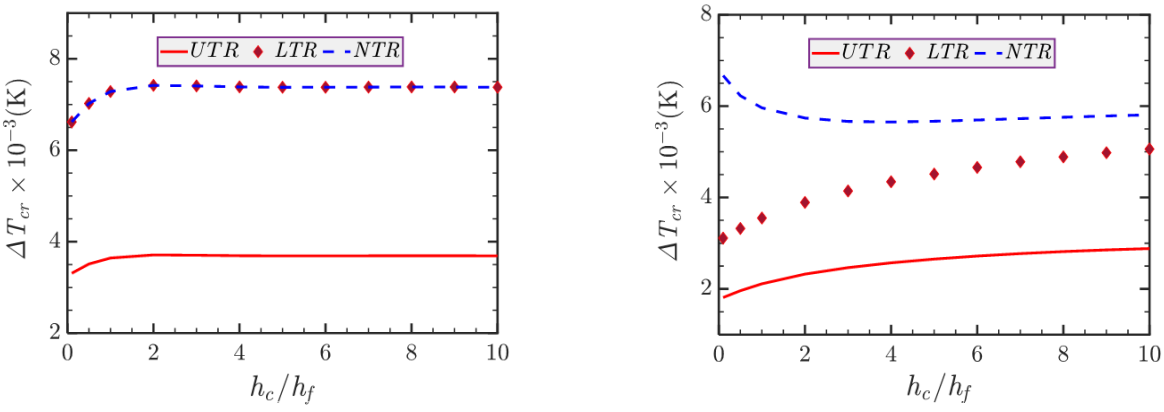

(a) FGM-FS I (b) FGM-FS II

Figure 7. The critical buckling temperature $\Delta T_{cr} \times 10^{-3}$ (in K) of the sandwich beams with respect to h_c/h_f for different temperature distributions (TBT, $L/h = 10$, $k = 2$, $e_o = 0.8$, CC$^{(II)}$)

4. Summary and conclusions

In this study, four typical beam models, which are the classical, first-order, third-order, and quasi-3D theories, are presented for the buckling of sandwich beams with a foam core subjected to either thermal or mechanical loading. Two types of sandwich beams, whose layers are constructed as FGM face-FG foam core-FGM face (FGM-FS I) and FGM face-FG foam core-isotropic face (FGM-FS II), are considered. These beam types satisfy the smooth variation of material properties over the beam depth. Three types of temperature distribution, i.e., UTR, LTR, and NTR, are considered. The trigonometric admissible functions-based Ritz method is adopted to discretize the governing equations for the approximate solution. The convergence is tested, and the accuracy of the study is confirmed. The effects of beam theories, material distribution, span-to-height ratio, temperature rises, porosity coefficient, boundary conditions, and layer thickness ratio on the buckling of the beams are numerically examined. Based on various numerical investigations, it is revealed that

(1) The critical buckling load and the critical buckling temperature predicted by different beam theories are significantly different for thick beams.

(2) The critical buckling temperature of the quasi-3D theory is distinctly different and smaller than that of the third-order beam theory, even for thin beams. However, these features are reversed for the critical buckling load.

(3) The critical buckling load usually decreases, but the critical buckling temperature increases/increases initially and then decreases as the porosity coefficient e_o increases.

(4) The critical buckling load usually decreases, but the critical buckling temperature increases/increases and then decreases slightly/decreases initially then increases slightly as the layer thickness ratio h_c/h_f of the beams increases.

(5) For the beam with a symmetry of layer structure, i.e., FGM-FS I, the critical buckling temperatures for LTR and NTR are almost identical.

(6) Both the critical buckling load and the critical buckling temperature of the beams increase as the power-law index k increases.

(7) The FGM-FS I beam performs much better than FGM-FS II in both mechanical and thermal buckling behavior.

This study is limited to the thermal buckling analysis of FGM-FS beams with temperature-independent material properties, which may influence the quantitative accuracy of the predicted critical buckling temperatures at high temperatures. In addition, the porous core is modeled using a symmetric cosine-based porosity distribution, which provides an idealized representation of the graded foam core and is primarily intended to capture the global structural behavior of the sandwich beam. Future work will incorporate temperature-dependent material behavior and extend the analysis to other types of porosity distributions or FGM-FS structures.

Acknowledgment

This work is funded by the Hanoi University of Civil Engineering (HUCE) under grant number 01-2026/KHXD-TC

References

[1] Ebrahimi, F. (2016). *Advances in Functionally Graded Materials and Structures*. BoD-Books on Demand.

[2] Udupa, G., Rao, S. S., Gangadharan, K. V. (2014). Functionally Graded Composite Materials: An Overview. *Procedia Materials Science*, 5:1291–1299.

[3] Gupta, A., Talha, M. (2015). Recent development in modeling and analysis of functionally graded materials and structures. *Progress in Aerospace Sciences*, 79:1–14.

[4] Sayyad, A. S., Ghugal, Y. M. (2019). Modeling and analysis of functionally graded sandwich beams: a review. *Mechanics of Advanced Materials and Structures*, 26(21):1776–1795.

[5] Vo, T. P., Thai, H.-T., Nguyen, T.-K., Maheri, A., Lee, J. (2014). Finite element model for vibration and buckling of functionally graded sandwich beams based on a refined shear deformation theory. *Engineering Structures*, 64:12–22.

[6] Şimşek, M. (2016). Buckling of Timoshenko beams composed of two-dimensional functionally graded material (2D-FGM) having different boundary conditions. *Composite Structures*, 149:304–314.

[7] Nguyen, T.-K., Vo, T. P., Nguyen, B.-D., Lee, J. (2016). An analytical solution for buckling and vibration analysis of functionally graded sandwich beams using a quasi-3D shear deformation theory. *Composite Structures*, 156:238–252.

[8] Sayyad, A. S., Ghugal, Y. M. (2020). On the buckling analysis of functionally graded sandwich beams using a unified beam theory. *Journal of Computational Applied Mechanics*, 51(2):443–453.

[9] Le, C. I., Le, N. A. T., Nguyen, D. K. (2021). Free vibration and buckling of bidirectional functionally graded sandwich beams using an enriched third-order shear deformation beam element. *Composite Structures*, 261:113309.

[10] Vo, T. P., Thai, H.-T., Nguyen, T.-K., Inam, F., Lee, J. (2015). A quasi-3D theory for vibration and buckling of functionally graded sandwich beams. *Composite Structures*, 119:1–12.

[11] Jiao, Z., Wang, G., Xu, R., Chen, W., Reddy, J. N. (2024). Free vibration and buckling analysis of functionally graded beams using the DMCDM. *Composite Structures*, 332:117905.

[12] Kiani, Y., Eslami, M. R. (2010). Thermal buckling analysis of functionally graded material beams. *International Journal of Mechanics and Materials in Design*, 6(3):229–238.

[13] Esfahani, S. E., Kiani, Y., Eslami, M. R. (2013). Non-linear thermal stability analysis of temperature dependent FGM beams supported on non-linear hardening elastic foundations. *International Journal of Mechanical Sciences*, 69:10–20.

[14] Ghiasian, S. E., Kiani, Y., Eslami, M. R. (2013). Dynamic buckling of suddenly heated or compressed FGM beams resting on nonlinear elastic foundation. *Composite Structures*, 106:225–234.

[15] She, G.-L., Yuan, F.-G., Ren, Y.-R. (2017). Thermal buckling and post-buckling analysis of functionally graded beams based on a general higher-order shear deformation theory. *Applied Mathematical Modelling*, 47:340–357.

[16] Nguyen, T.-K., Nguyen, B.-D., Vo, T. P., Thai, H.-T. (2017). Hygro-thermal effects on vibration and thermal buckling behaviours of functionally graded beams. *Composite Structures*, 176:1050–1060.

[17] Aria, A. I., Friswell, M. I. (2019). Computational hygro-thermal vibration and buckling analysis of functionally graded sandwich microbeams. *Composites Part B: Engineering*, 165:785–797.

[18] Chen, W.-R., Chen, C.-S., Chang, H. (2020). Thermal Buckling Analysis of Functionally Graded Euler-Bernoulli Beams with Temperature-dependent Properties. *Journal of Applied and Computational Mechanics*, 6(3):457–470.

[19] Daikh, A. A., Guerroudj, M., El Adjrami, M., Megueni, A. (2020). Thermal Buckling of Functionally Graded Sandwich Beams. *Advanced Materials Research*, 1156:43–59.

[20] Nguyen, T.-N., Nguyen, N.-D. (2025). A Ritz-type solution for free vibration and buckling analysis of functionally graded beams under hygro-thermal environment. *Structures*, 73:108392.

[21] Hung, D. X., Truong, H. Q. (2018). Free vibration analysis of sandwich beams with FG porous core and FGM faces resting on Winkler elastic foundation by various shear deformation theories. *Journal of Science and Technology in Civil Engineering – NUCE*, 12(3):23–33.

[22] Chinh, T. H., Tu, T. M., Duc, D. M., Hung, T. Q. (2021). Static flexural analysis of sandwich beam with functionally graded face sheets and porous core via point interpolation meshfree method based on polynomial basic function. *Archive of Applied Mechanics*, 91(3):933–947.

[23] Mu, L., Zhao, G. (2016). Fundamental Frequency Analysis of Sandwich Beams with Functionally Graded Face and Metallic Foam Core. *Shock and Vibration*, 2016:3287645.

[24] Wang, Y., Zhou, A., Fu, T., Zhang, W. (2020). Transient response of a sandwich beam with functionally graded porous core traversed by a non-uniformly distributed moving mass. *International Journal of Mechanics and Materials in Design*, 16(3):519–540.

[25] Hung, T. Q., Duc, D. M., Tu, T. M. (2022). Static Behavior of Functionally Graded Sandwich Beam with Fluid-Infiltrated Porous Core. In *Modern Mechanics and Applications*, Springer, 691–706.

[26] Hung, T. Q., Duc, D. M., Tu, T. M. (2023). Free and Forced Vibration Characteristics of Functionally Graded Sandwich Beam with GPL-Reinforced Porous Core. In *Proceedings of The 17th East Asian-Pacific Conference on Structural Engineering and Construction, 2022*, Singapore, Springer Nature Singapore, 1432–1452.

[27] Wattanasakulpong, N., Chaikittiratana, A. (2025). A comprehensive study on bending, buckling and vibration of sandwich beams made of FG-GPLRC faces and FGP core using a quasi-3D theory. *Structures*, 74:108561.

[28] Mohamed, I., Kahya, V., Şimşek, S. (2025). Ritz-type quasi-3D solution for free vibration and buckling of functionally graded sandwich beams with porous core resting on a two-parameter elastic foundation. *Arabian Journal for Science and Engineering*, 50(16):13343–13367.

[29] Eiadtrong, S., Nguyen, T. N., Wattanasakulpong, N. (2024). Nonlinear vibration of sandwich beams made of FGM faces and FGP core under multiple moving loads using a quasi-3D theory. *Engineering Structures*, 316:118575.

[30] Chen, D., Kitipornchai, S., Yang, J. (2016). Nonlinear free vibration of shear deformable sandwich beam with a functionally graded porous core. *Thin-Walled Structures*, 107:39–48.

[31] Setoodeh, A., Ghorbanzadeh, M., Malekzadeh, P. (2012). A two-dimensional free vibration analysis of functionally graded sandwich beams under thermal environment. *Proceedings of the Institution of Mechanical Engineers, Part C: Journal of Mechanical Engineering Science*, 226(12):2860–2873.

[32] Reddy, J. N. (1984). A Simple Higher-Order Theory for Laminated Composite Plates. *Journal of Applied Mechanics*, 51(4):745–752.

[33] Zhang, D.-G. (2013). Nonlinear bending analysis of FGM beams based on physical neutral surface and high order shear deformation theory. *Composite Structures*, 100:121–126.

[34] Yaghoobi, H., Fereidoon, A. (2014). Mechanical and thermal buckling analysis of functionally graded plates resting on elastic foundations: An assessment of a simple refined nth-order shear deformation

theory. *Composites Part B: Engineering*, 62:54–64.

[35] Zenkour, A. M., Sobhy, M. (2011). Thermal Buckling of Functionally Graded Plates Resting On Elastic Foundations Using the Trigonometric Theory. *Journal of Thermal Stresses*, 34(11):1119–1138.

[36] Zenkour, A. M., Radwan, A. F. (2019). Hygrothermo-mechanical buckling of FGM plates resting on elastic foundations using a quasi-3D model. *International Journal for Computational Methods in Engineering Science and Mechanics*, 20(2):85–98.

[37] Wang, C. M., Ke, L. L., Roy Chowdhury, A. N., Yang, J., Kitipornchai, S., Fernando, D. (2017). Critical examination of midplane and neutral plane formulations for vibration analysis of FGM beams. *Engineering Structures*, 130:275–281.

[38] Trinh, L. C., Vo, T. P., Osofero, A. I., Lee, J. (2016). Fundamental frequency analysis of functionally graded sandwich beams based on the state space approach. *Composite Structures*, 156:263–275.

[39] Tang, H., Li, L., Hu, Y. (2018). Buckling analysis of two-directionally porous beam. *Aerospace Science and Technology*, 78:471–479.

[40] Kitipornchai, S., Chen, D., Yang, J. (2017). Free vibration and elastic buckling of functionally graded porous beams reinforced by graphene platelets. *Materials & Design*, 116:656–665.